Nuclear Instruments and Methods in Physics Research A 845 (2017) 47–51

Contents lists available at ScienceDirect

Nuclear Instruments and Methods in Physics Research A

journal homepage: www.elsevier.com/locate/nima

Tracking in 4 dimensions

N. Cartiglia [a,*], R. Arcidiacono [a,g], B. Baldassarri [a,c], M. Boscardin [b,d], F. Cenna [a,e], G. Dellacasa [a,e], G.-F. Dalla Betta [b,f], M. Ferrero [a,e], V. Fadeyev [h], Z. Galloway [h], S. Garbolino [a,e], H. Grabas [h], V. Monaco [a,e], M. Obertino [a,e], L. Pancheri [b,f], G. Paternoster [b,d], A. Rivetti [a], M. Rolo [a], R. Sacchi [a,e], H. Sadrozinski [h], A. Seiden [h], V. Sola [a,e], A. Solano [a,e], A. Staiano [a], F. Ravera [a,e], A. Zatserklyaniy [h]

[a] INFN, Torino, Italy
[b] TIFPA INFN, Trento, Italy
[c] UCL, London, England
[d] Fondazione Bruno Kessler, Trento, Italy
[e] Università di Torino, Italy
[f] Università di Trento, Italy
[g] Università del Piemonte Orientale, Italy
[h] University of California, Santa Cruz, CA 95064, USA

ARTICLE INFO

Article history:
Received 12 March 2016
Received in revised form
17 May 2016
Accepted 20 May 2016
Available online 3 June 2016

Keywords:
Tracking
UFSD
LGAD
Ultrafast
Particles
Silicon

ABSTRACT

In this contribution we will review the progresses toward the construction of a tracking system able to measure the passage of charged particles with a combined precision of ~10 ps and ~10 μm, either using a single type of sensor, able to concurrently measure position and time, or a combination of position and time sensors.

1. The effect of timing information

The inclusion of timing information in the structure of a recorded event has the capability of changing the way we design experiments, as this added dimension dramatically improves the reconstruction process. Depending on the type of sensors that will be used, timing information can be available at different stages in the reconstruction of an event, for example (i) at tracking reconstruction, if timing is associated to each point or (ii) during the event reconstruction, if timing information is associated to each track. In the first case, the 4th dimension brings a simplification already in the reconstruction algorithm as only time-compatible hits are used in the pattern recognition phase, however the electronics is very demanding as it needs to be able to accurately measure timing in each pixel. The second case is simpler as it requires the implementation of a dedicated timing layer, either inside or outside the main silicon tracker volume, to assign the timing information to each crossing track without changing the vast majority of the tracker hardware. The timing information can then be used to improve Level 1 trigger decisions, as it can be obtained faster than tracking reconstruction, and to separate events with overlapping vertices.

Considering a specific situation, at HL-LHC the number of events per bunch crossing will be of the order of 150–200, with an average distance between vertexes of 500 micron and a timing rms spread of 150 ps. Considering a vertex separation resolution of 250–300 micron along the beam direction (present resolution for CMS and ATLAS), there will be 10–15% of vertexes composed by two overlapping events. This overlap will cause a degradation in the precision of the reconstructed variables, and lead to loss of events. Examples where timing information is crucial to avoid loss of measuring accuracy are a) the correct assignment of each particle to its event when two interactions overlap, b) the

* Corresponding author.
E-mail address: cartiglia@to.infn.it (N. Cartiglia).

http://dx.doi.org/10.1016/j.nima.2016.05.078
0168-9002/

identification of the correct $H \rightarrow \gamma\gamma$ vertex , and c) the association of displaced tracks to the correct vertex. We can therefore conclude that timing information at HL-LHC is equivalent of having additional luminosity.

2. Time-tagging detectors

In the following we will use a simplified model to explore the timing capabilities of various detectors (for a review of current trends in electronics see for example [1]): the sensor, thought as a capacitor (C_{Det}) with a current source in parallel, is readout by a pre-amplifier that shapes the signal. The pre-amplifier's output is then compared to a fixed threshold (V_{Th}) to determine the time of arrival. The time resolution σ_t can be expressed as the sum of several terms: (i) Jitter, (ii) Landau Time Walk (iii) Landau noise due to shape variation, (iv) signal distortion, and (v) TDC binning:

$$\sigma_t^2 = \sigma_{jitter}^2 + \sigma_{Land.\ TW}^2 + \sigma_{Land.\ noise}^2 + \sigma_{Distortion}^2 + \sigma_{TDC}^2. \quad (1)$$

We will assume in the following two simplifications:

- We consider the effect of time walk (see [2] for details) compensated by an appropriate electronic circuit (either Constant Fraction Discriminator or Time over Threshold). With this assumption, the effect of Landau variations in signal amplitude are compensated, but not that of shape variation. This second contribution is indicated as Landau noise ($\sigma_{Land.\ Noise}^2$) in Eq. (1).
- The contribution of TDC binning to be below 10 ps and therefore negligible.

2.1. Jitter

The jitter term represents the time uncertainty caused by the early or late firing of the comparator due to the presence of noise. It is directly proportional to the noise N and it is inversely proportional to the slope of the signal around the value of the comparator threshold. Assuming a constant slope we can write $dV/dt = S/t_r$ and therefore:

$$\sigma_J = \frac{N}{dV/dt} = \frac{t_r}{S/N}. \quad (2)$$

2.2. Landau fluctuations: time walk and Landau noise

The ultimate limit to signal uniformity is given by the physics governing energy deposition: the charge distribution created by an ionizing particle crossing a sensor varies on an event-by-event basis. These variations not only produce an overall change in signal magnitude, which is at the root of the time walk effect (that we assumed perfectly corrected by electronics), but also produce an irregular current signal (Landau noise). The left part in Fig. 1 shows 2 examples of the simulated [3] energy deposition of a minimum ionizing particle, while the right part the associated generated current signals and their components: the variations are rather large and they can severely degrade the achievable time resolution.

2.3. Signal distortion: weighting field and drift velocity

In every particle detector, the shape of the induced current signal can be calculated using Ramo's [4] theorem that states that the current induced by a charge carrier is proportional to its electric charge q, the drift velocity v and the weighting field E_w: $i(t) \propto qvE_w$. This equation indicates two key points in the design of sensors for accurate timing. First, the drift velocity needs to be constant throughout the volume of the sensor. Non-uniform drift velocities induce variations in signal shape as a function of the hit position, Fig. 2a, spoiling the overall time resolution. The easiest

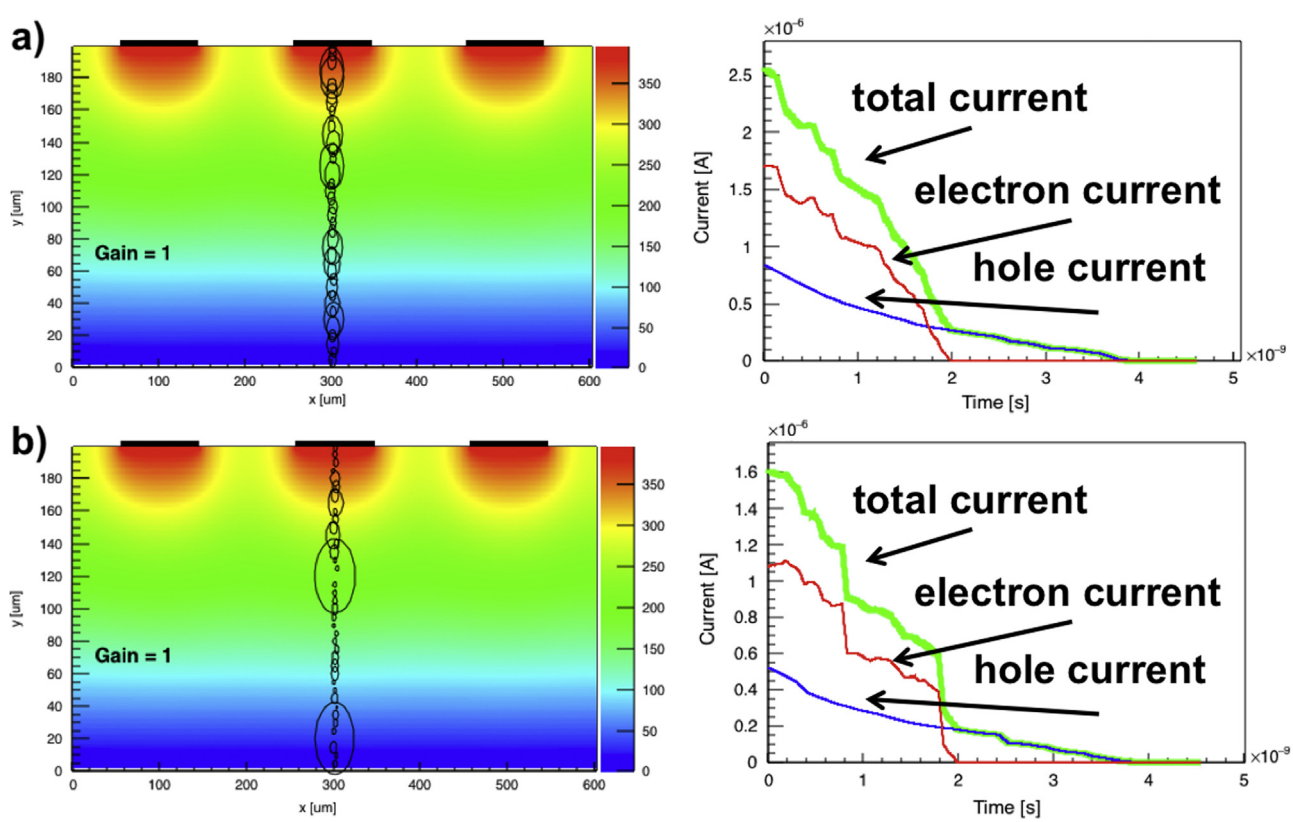

Fig. 1. a) Energy deposits in a silicon detector with gain =1, and (b) the corresponding current signals.

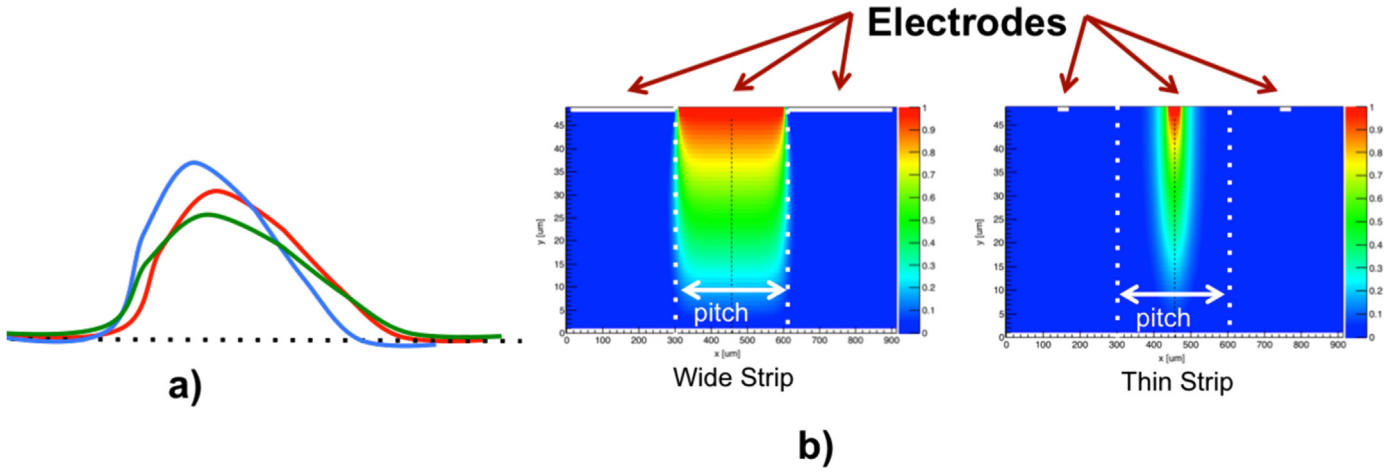

Fig. 2. a) Effect of velocity variation on the signal shape and b) weighting field for two configurations: (left) wide strips, (right) thin strips.

way to obtain uniform drift velocity throughout the sensor is to have an electric field high enough to move the carriers with saturated drift velocity. Second, strips need to have the width very similar to the pitch, and these two dimensions need to be larger than the sensor thickness: width ~ pitch≫thickness. These requirements are making the weighting field very uniform along the strip width, as shown in Fig. 2b.

2.4. Roadmap

The integration of time-tagging capabilities into a position sensor produces a steep increase in system complexity. Part of this complexity can be addressed by very smart architectures, new technological nodes (for example 65 nm) allowing higher circuit densities and new chip designs. However having sensors and electronics built on separated substrates will ultimately limit the level of integration and drive the cost. Most likely the real turning point of 4D tracking will happen when monolithic technology will be mature enough to allow integrating the sensor and the electronics in the same substrate, reducing interconnections and keeping the capacitance of each sensor low.

3. Possible detectors for a 4D tracker

Assuming that a 4D tracker should maintain the key aspects of current 3D tracker designs, then the type of possible detectors is limited by material budget consideration to semiconductor devices, mostly silicon and diamond. Assuming some overall design aspects equal (saturated drift velocity, weighting field, manufacturing capability, cost), the key quantity to be minimized by every detector is the jitter term expressed by equation Eq. (2). We will here briefly review 4 possible approaches, concentrating on Ultra-Fast Silicon Detectors.

3.1. Silicon detectors

Standard silicon detectors can be used in timing applications, provided the sensor geometry is appropriate. Currently the NA62 experiment [5] is employing a track-timing detector, the so called GiGatracker, that uses 200-micron thick sensors with 300-micron pixels. The expected time resolution is around $\sigma_t \sim 150$ ps. Employing an extremely low noise new circuit [6], a resolution of $\sigma_t \sim 105$ ps has been reached using a 100-micron thick, 2 mm square pad sensor. Standard silicon sensors have therefore the capability of reaching good time resolutions, however it is rather difficult to reach resolutions better than σ_t~80–100 ps given their small signal.

3.2. Diamond detectors

Diamond has a large energy gap therefore it has almost no leakage current, it is radiation resistant, it has a small dielectric constant, so the capacitance is low, and carriers have high mobility. The main drawback is the small signal amplitude (due to the large energy gap), and the limited commercial offer. There are currently two techniques to increase the signal amplitude: a) stacking sensors - overlapping several sensors that are read in parallel - and b) grazing - placing the sensors with the surface parallel to the direction of the particle. Diamond detectors have been therefore used successfully as time tagging sensors since they have low noise (due to their small capacitance), and a large dV/dt. The best result achieved so far has been $\sigma_t \sim 100$ ps, obtained by the TOTEM collaboration. Given the difficulties of large scale production, diamond detectors are therefore ideally suited for small area sensors in high radiation environments.

3.3. APD – Avalanche PhotoDiode

APD can successfully be employed in the detection of charged particles. APD are normally quite thin, 30–50 micron, so the initial number of charge carriers generated by a MIP particles is rather small, 2–3000 e/h pairs, however their signal is very large since they have a gain of the order of 50–500. Given the short drift distance, the signal is very short and steep, with a very large dV/dt: APD have therefore excellent time resolution, of the order of $\sigma_t \sim 30$ ps. The same quality that makes APD very good timing sensors, high gain, is however also causing drawbacks: (i) when irradiated, APD have very high Shot noise (due to the multiplication of the leakage current, see Section 3.4.2), (ii) they cannot be easily segmented, and (iii) they suffer from electric breakdown. APD are therefore a very good choice for single pad systems in low radiation environments. Their use as segmented sensors in high radiation experiments still need to be demonstrated.

3.4. LGAD – Low-Gain Avalanche Detectors

LGAD is a new concept in silicon detector design, merging the best characteristics of standard silicon sensors with the main feature of APDs. The overarching idea is to design silicon detectors with signals that are a factor of 10 higher than those of standard sensors, however without the problems connected with the APD

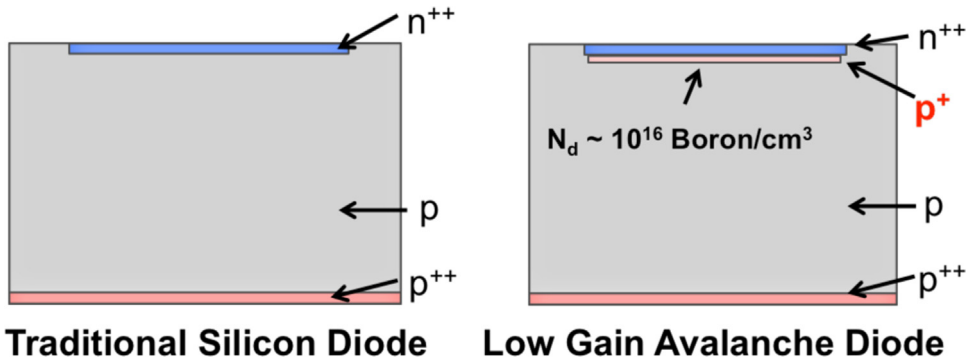

Fig. 3. Schematic of a traditional silicon diode (left) and of a Low-Gain Avalanche Diode (right).

high gain [7–9]. Charge multiplication in silicon sensors happens when the charge carriers are in electric fields of the order of $E \sim 300$ kV/cm. Under this condition the electrons (and to less extent the holes) acquire sufficient kinetic energy that are able to generate additional e/h pairs. A field value of 300 kV/cm is obtained by implanting an appropriate charge density that locally generates very high fields ($N_D \sim 10^{16}/\text{cm}^3$). The gain has an exponential dependence on the electric field $N(l) = N_o e^{\alpha(E)l}$, where $\alpha(E)$ is a strong function of the electric field and l is the path length inside the high field region. The additional doping layer present at the $n-p$ junction in the LGAD design, Fig. 3, generates the high field necessary to achieve charge multiplication. We have developed a full simulation program, WF2 [3], to study the property of signal formation in silicon detectors and the effect of gain. According to WF2, LGAD have the potentiality of replacing standard silicon sensors in almost every application, with the added advantage of having a large dV/dt and therefore being able to measure time accurately. In the following, we will use the name of "Ultra-Fast Silicon detectors" (UFSD) to indicate LGAD sensors optimized for timing performances.

3.4.1. UFSD: landau noise

With WF2 we have studied in details the effect of Landau noise on time resolution, Fig. 4. The picture shows several important effects: (i) Landau noise sets a physical limit to the precision of a given sensor which is of the order of 20 ps in thin sensors, and much larger for thicker sensors, (ii) Landau noise is minimized by setting the comparator threshold as low as possible, and (iii) thin detectors are less prone to Landau noise.

3.4.2. UFSD: shot noise and irradiation effects

Shot noise arises when charge carriers cross a potential barrier, as it happens in silicon sensors. Assuming an electronics integration time τ, the equivalent noise charge is given by: $ENC_{Shot} = \sqrt{I_{Bulk}/(2e)\tau}$, where I_{Bulk} is the leakage current generated in the bulk collected by the read-out electrode. In sensors such as UFSD or APD this effect is enhanced by the gain and for this reason

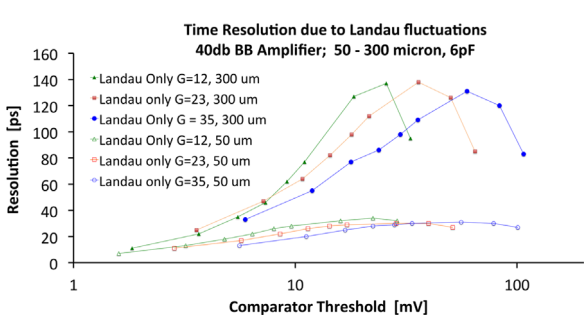

Fig. 4. Effect of Landau noise on time resolution. Best results are obtained for thin sensors with a low comparator threshold.

Shot noise can be the dominant source of noise. Moreover, when carriers undergo multiplication, there is an additional mechanism that enhances Shot noise: multiplication is a stochastic process, therefore some carries multiply more than others, causing a noise increase, the so called *excess noise factor* (ENF). The expression for Shot noise in device with gain is therefore:

$$ENC_{Shot} = \sqrt{\frac{I_{Bulk} M^2 M^x}{2e}\tau} \tag{3}$$

where M is the gain value, and x is the excess noise index. ENF causes a very peculiar effect: in device with gain, as the gain increases the signal-to-noise ratio (S/N) becomes smaller since Shot noise increases faster ($\propto \sqrt{M^{2+x}}$) than the signal ($\propto M$). In order to obtain a beneficial effect from the gain mechanism is therefore necessary to have a gain value small enough (gain ≤ 20) such that the signal increases while the noise increment is still in the shadow of the electronic noise floor. Fig. 5 shows the value of Shot noise for a 4 mm^2 50-micron thick silicon sensor as a function of radiation dose, assuming a 2-ns long integration time. In the plots the electronic noise is assumed to be 450 ENC. Fig. 5a demonstrates the dramatic effect of gain on Shot noise, while Fig. 5b the effect of temperature (leakage current decreases a factor of 2 every 7°). Fig. 5 demonstrates that Shot noise can become the most important source of noise for irradiated sensors with gain, and suggests that small volumes and low temperature can keep this effect under control provided the gain is low enough.

Radiation damage causes three main effects: (i) decrease of charge collection efficiency [10], (ii) increase of leakage current, causing Shot noise see 3.4.2, and (iii) changes in doping concentration. UFSD sensors have shown a decrease of gain values for fluences above 10^{14} n_{eq}/cm^2, with a complete disappearance of the gain at 10^{15} n_{eq}/cm^2. This effect has not been understood yet, but there are two possible explanations: (i) an inactivation of acceptors due to radiation defects [11], and/or (ii) a dynamic reduction of the gain layer doping due to charge trapping.

3.4.3. UFSD: testbeam results and extrapolation

We have performed several beam tests to validate the design of UFSD sensors. The results, together with simulation predictions, are shown in Fig. 6. The best resolution for 300-micron thick sensors is $\sigma_t \sim 120$ ps, equally due to, according to simulation, jitter and Landau noise contributions; a dramatic improvement is predicted for thin sensors, reaching a resolution of $\sigma_t \sim 30$ ps for 50-micron thick sensors.

4. Conclusions and outlook

Tracking in 4 dimensions requires the development of dedicated sensors and associated electronics. Several approaches are

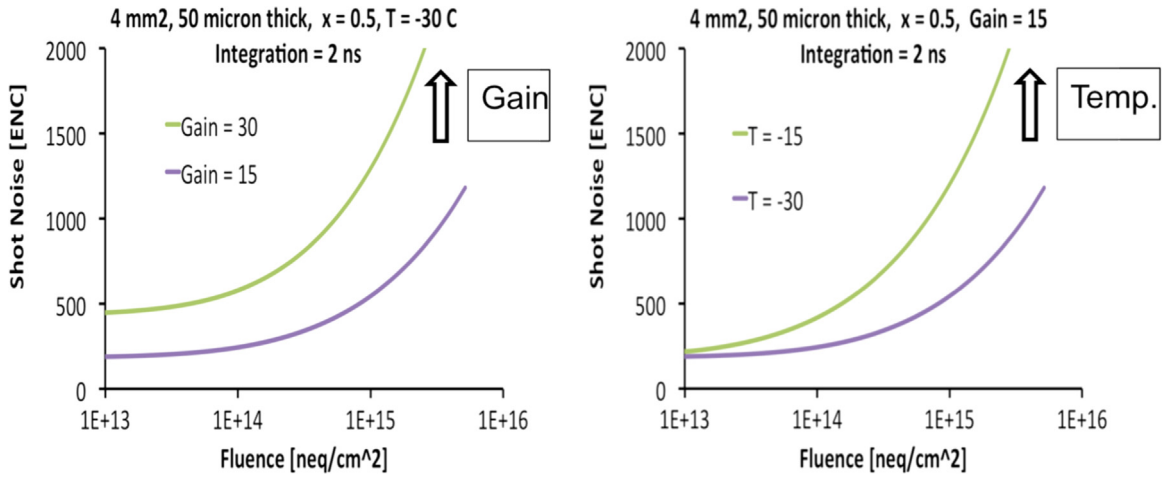

Fig. 5. (a) Shot noise increase as a function of fluence for two different gain values. (b) Shot noise increase as a function of fluence for two different temperature values.

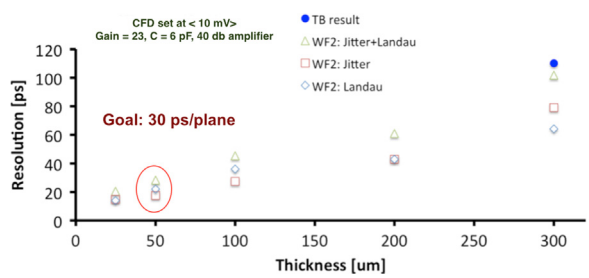

Fig. 6. Beam test results for 300-micron UFSD sensors, and extrapolation to thin sensors. For each thickness, the predictions obtained by the WF2 program for the Landau noise and the jitter term are also shown.

currently being investigated (Diamond, UFSD, APD, Silicon), and each one is responding to specific experimental requests. The most important points to achieve excellent time resolution are: (i) high field to have saturated velocity and minimize signal distortion, (ii) geometries as similar as possible to parallel plate capacitors, offering uniform electric and weighting fields, (iii) high velocity carriers, to have large dV/dt, (iv) low capacitance, to minimize noise and therefore jitter, and (v) small volumes, to minimize leakage current and therefore Shot noise. The design of UFSD adds two points: low gain (large signal, minimum excess noise, easier segmentation, low power) and thin sensors (maximum dV/dt, low leakage current, small trapping).

Acknowledgments

We acknowledge the following funding agencies: Horizon 2020 under the program ERC Adv Grants 669529 Ministero degli Affari Esteri, Italy, MAE (grant name: UFSD); U.S. Department of Energy Grant no. DE-SC0010107.

References

[1] A. Rivetti, CMOS: Front-End Electronics for Radiation Sensors, CRC Press, 2015, ISBN 9781466563100.
[2] N. Cartiglia, et al., Design optimization of ultra-fast silicon detectors, Nucl. Instrum. Methods A 796 (2015) 141–148, http://dx.doi.org/10.1016/j.nima.2015.04.025.
[3] F. Cenna, et al., Weightfield2: a fast simulator for silicon and diamond solid state detector, NIM A 796 (2015) 149–153.
[4] S. Ramo, Currents induced by electron motion, in: Proceedings of the IRE, vol. 27(9), 1939, pp. 584–585. http://dx.doi.org/10.1109/JRPROC.1939.228757.
[5] M. Perrin-Terrin, et al., The NA62 gigatracker, Pos. VERTEX2015 (2015) 016.
[6] M. Benoit, et al., 100 ps time resolution with thin silicon pixel detectors and a SiGe HBT amplifier, arXiv:1511.04231.
[7] G. Pellegrini, et al., Technology developments and first measurements of low gain avalanche detectors (lgad) for high energy physics applications, Nucl. Instrum. Methods 765A (2014) 12–16.
[8] G.-F.D. Betta, et al., Design and tcad simulation of double-sided pixelated low gain avalanche detectors, NIM A 796 (2015) 154–157.
[9] H.F.W. Sadrozinski, et al., Ultra-fast silicon detectors, Nucl. Instrum. Methods A 730 (2013) 226–231, http://dx.doi.org/10.1016/j.nima.2013.06.033.
[10] B. Baldassarri, et al., Signal Formation in irradiated silicon detectors., in: Proceedings of the 14th Vienna Conference on Instrumentation (VCI 2016), 2016.
[11] G. Kramberger, et al., Radiation effects in low gain avalanche detectors after hadron irradiations, JINST 10 (07) (2015) P07006, http://dx.doi.org/10.1088/1748-0221/10/07/P07006.